Computer Science Technical Report TR-07-30 (989) August 22, 2007

Adrian Sandu and
Emil M. Constantinescu

"Multirate explicit Adams methods for time integration of conservation laws"

Computer Science Department
Virginia Polytechnic Institute and State University
Blacksburg, VA 24060
Phone: (540)-231-2193
Fax: (540)-231-6075
Email: {sandu, emconsta}@cs.vt.edu
http://eprints.cs.vt.edu

Multirate explicit Adams methods for time integration of conservation laws *

Adrian Sandu ‡ Emil M. Constantinescu †

August 22, 2007

Abstract

This paper constructs multirate linear multistep time discretizations based on Adams-Bashforth methods. These methods are aimed at solving conservation laws and allow different timesteps to be used in different parts of the spatial domain. The proposed family of discretizations is second order accurate in time and has conservation and linear and nonlinear stability properties under local CFL conditions. Multirate timestepping avoids the necessity to take small global timesteps – restricted by the largest value of the Courant number on the grid – and therefore results in more efficient computations. Numerical results obtained for the advection and Burgers' equations confirm the theoretical findings.

1 Introduction

Conservation laws are of great practical importance as they model diverse physical phenomena that appear in mechanical and chemical engineering, aeronautics, astrophysics, meteorology, environmental sciences, etc. Representative examples are gas dynamics, shallow water flow, groundwater flow, non-Newtonian flows, traffic flows, advection and dispersion of contaminants, etc.

Conservative high resolution methods with explicit time discretization have gained widespread popularity for numerically solving conservation laws [25]. Stability requirements limit the temporal step size, with the

*This work was supported by the National Science Foundation through award NSF CCF-0515170.

†Department of Computer Science, Virginia Polytechnic Institute and State University, Blacksburg, VA 24061, Tel. +1 540 231 2193 (asandu@cs.vt.edu,emconsta@cs.vt.edu).

‡Corresponding author.

upper bound being determined by the ratio of the temporal and spatial meshes and the magnitude of the wave speed. The timestep for the entire domain is restricted by the finest (spatial) mesh resolution or by the highest wave velocity, and is typically (much) smaller than necessary to accurately represent other variables in the computational domain.

Implicit, unconditionally stable timestepping algorithms allow large global timesteps; however, this approach requires the solution of large (non)linear systems of equations. Moreover, the quality of the solution, as given by a maximum principle, may not be preserved with high order implicit schemes unless the timestep is also restricted by a CFL-like condition [10].

In multirate time integration methods, the timestep can vary across the spatial domain and has to satisfy the CFL condition only locally, resulting in substantially more efficient overall computations. We follow the method of lines (MOL) framework, where the temporal and spatial discretizations are independent.

The development of multirate integration for conservation laws is challenging due to the conservation and stability constraints that need to be simultaneously satisfied. The algorithms used in the solution of conservation laws need to preserve the system invariants. Furthermore, the integration schemes need to account for non-smooth solutions (e.g., shock waves or other discontinuous behavior). In such cases, strong-stability-preserving (SSP) numerical methods which satisfy nonlinear stability requirements are necessary to avoid certain types of nonphysical behavior (e.g., spurious oscillations [10]).

Early efforts to develop multirate Runge-Kutta methods are due to Rice [28] and Andrus [1, 2]. Gear and Wells [9] pioneered the multirate linear multistep approach. Multirate versions of many of the traditional timestepping schemes have been proposed in the literature, including linear multistep [9, 18], extrapolation [8], Runge-Kutta [6, 11, 20, 21], Rosenbrock-Wanner [3, 12], waveform relaxation [29], and others.

In a previous study [6] we have developed SSP multirate Runge-Kutta methods. In the current work we focus our attention on multirate linear multistep time integration schemes for the simulation of PDEs. Specifically, we study the Adams-Bashforth methods. The strong stability properties of single-rate AB methods have been studied by Hundsdorfer et al. [16, 17] and they rely on the ODE contractivity theory developed in [19, 23, 24].

In this paper we extend the Adams-Bashforth methods to multirate methods that are second order accurate and conservative. Note that previous multirate approaches lead to first order accuracy due to the interface treatment [9, 18].

This paper is structured as follows: Section 2 presents the construction

of the multirate time integrators from single rate schemes. Numerical results for linear and nonlinear conservation laws are presented in Section 3. Conclusions and future research directions are given in Section 4.

2 Multirate Explicit Adams Methods

Consider the following initial value problem

$$\begin{aligned} & w'(t,x) = F\Big(w(t,x)\Big), \ \text{ with } w(t_0,x) = w_0(x)\,, \\ & \text{on} \quad x \in \Psi \subset (-\infty,\infty)\,,\ t \geq t_0\,, \end{aligned} \tag{1}$$

solved with the explicit k-step Adams method [13, Ch. III]:

$$w_n = w_{n-1} + h\sum_{i=1}^{k} \beta_i F\Big(w_{n-i}\Big)\,. \tag{2}$$

The following notation will be used to denote the discrete solution $(w_n)_i = w(t_n, x_i)$, with $n > 0$ and $x_i \in \Omega$, where Ω is the discrete spatial domain. The total variation (TV) semi-norm $\|\circ\|_{TV}$ of the numerical solution is defined as

$$\|w_n\|_{TV} = \sum_i |(w_n)_{i+1} - (w_n)_i|\,,\ x_i \in \Omega\,,$$

A numerical method is called total variation diminishing (TVD) [14] if

$$\|w_n\|_{TV} \leq \|w_{n-1}\|_{TV}\,, \forall n \geq 1\,.$$

A numerical method is called total variation bounded (TVB) (see [31]) if

$$\|w_n\|_{TV} \leq B\,,\ \forall n \geq 0\,,\ B > 0\,.$$

In this case some bounded total variation increase is allowed. TVD methods are also TVB.

Methods that satisfy

$$\|w_n\| \leq \|w_{n-1}\|\,, \quad \forall n \geq 1\,, \tag{3}$$

for some norm or the TV semi-norm are called strong-stability-preserving.

Under a suitable timestep restriction, with an appropriate initialization, and with adequate β coefficients, the method (2) is strong stability preserving [17].

The idea of multirate timestepping is to take different timesteps for different components to achieve the target accuracy. Slower components

are integrated using larger step sizes. The large step sizes are integer multiple of the small step sizes. All steps are synchronized every largest timestep in order to obtain the desired overall accuracy. In (1) the solution w is separated explicitly in the slow (y) components and the fast (z) ones. With $w^T = [y^T, z^T]^T$ system (1) becomes

$$\frac{d}{dt}\begin{bmatrix} y \\ z \end{bmatrix} = \begin{bmatrix} f(y,z) \\ g(y,z) \end{bmatrix}, \tag{4}$$

where $F(w) = F(y, z) = [f^T(y, z)\, g^T(y, z)]^T$ is the right hand side of (1) corresponding to the slow components (f) and the fast ones (g).

In the PDE context and using the method of lines to yield (4), y can represent variables on a coarse grid and z variables on the fine grid. An illustration is shown in Figure 1. In this case f is evaluated on y and formally on z; however, in practice f depends on z only in a "small" neighborhood of the $y - z$ interface (e.g., space discretization stencil length). Same argument holds for g with y interchanged with z. Therefore "away" from the interface, f depends only on the slow components and g depends only on the fast ones. This fact can be used to efficiently discretize (4) by choosing the appropriate time step for each component.

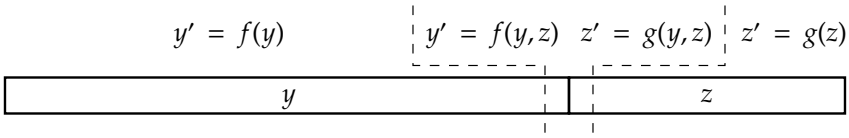

Figure 1: Illustration of the solution component partitioning. Away from the interface f is evaluated only on the slow components (y) and g is evaluated only on the fast components (z). In a narrow strip along the interface, f and g depend on both y and z.

In this paper we extend the explicit Adams methods (2) for the discretization of (1) to multirate Adams methods for the integration of partitioned systems of ordinary differential equations defined by (4). Each component is integrated with a different time step.

In what follows we denote by h the integration timestep for the fast components and by $H = mh$ the integration timestep for the slow components. There are m fast steps for each slow step. This means that the slow method updates the slow variables every m timesteps, while the fast method updates the components every timestep.

Let $n = M \cdot m$ be a multiple of m and consider that we have advanced the system to the time $t_{n-m} = t_0 + (n-m)h = t_0 + (M-1)m\,h$. The slow variables y_i are available for $i = n - m, n - 2m, n - 3m, \cdots$, while the fast variables

are available for all $0 \le i \le n-m$. Our goal is to advance the system from the time t_{n-m} to the time $t_n = t_0 + M\,m\,h$ using one step of length mh for the slow variables and m steps of length h for the fast variables.

We propose the following multirate version of the Adams method. For the slow variables: we take one large step using

$$y_n = y_{n-m} + h \sum_{i=1}^{k} \beta_i \left(\sum_{\ell=1}^{m} f\left(y_{n-i\cdot m}, z_{n-m+\ell-i}\right) \right). \tag{5}$$

For the fast variables we take m small steps (of length h):

$$\text{For } \ell = 1, \cdots, m: \quad z_{n-m+\ell} = z_{n-m+\ell-1} + h \sum_{i=1}^{k} \beta_i\, g\Big(y_{n-i\cdot m}, z_{n-m+\ell-i}\Big). \tag{6}$$

Remark 1. Inside the slow grid (and away from the fast-slow boundary) f depends only on y and (5) is the k-step Adams method applied with a step size of mh. Specifically, inside the slow grid (5) becomes

$$y_n = y_{n-m} + m\,h \sum_{i=1}^{k} \beta_i\, f\left(y_{n-i\cdot m}\right).$$

The slow components are evaluated once per macro-step inside the slow domain. Similarly, inside the fast grid (and away from the fast-slow boundary) g depends only on z and (6) are m consecutive steps the Adams method applied with the small step size h. Thus for hyperbolic problems with finite stencil space discretizations the method is truly multirate. In particular, slow fluxes are evaluated only once per macro-step except near the fast-slow interface.

Remark 2. The computational process is a fastest first strategy [9]. One first solves for the fast components (6), then uses them to compute the fluxes in (5).

Remark 3. The one-leg counterpart of the method (5)–(6) reads:

$$\text{For } \ell = 1, \cdots, m: \quad z_{n-m+\ell} = z_{n-m+\ell-1} + h\, g\left(\sum_{i=1}^{k} \beta_i y_{n-i\cdot m}, \sum_{i=1}^{k} \beta_i z_{n-m+\ell-i} \right) \tag{7}$$

$$y_n = y_{n-m} + h \sum_{\ell=1}^{m} f\left(\sum_{i=1}^{k} \beta_i\, y_{n-i\cdot m}, \sum_{i=1}^{k} \beta_i\, z_{n-m+\ell-i} \right). \tag{8}$$

Remark 4. The same "base" Adams method (2) is used for both fast and slow components in (5)-(6). In this approach, the scheme (5)-(6) can be used in a telescopic fashion. Thus this is not only a two-rate approach, but allows multiple time levels; e.g., for three (time scale) components, the method can accommodate the timesteps: H, H/m, and H/m^2.

2.1 Examples of Multirate Adams Methods

In applications we are mainly interested in $k = 2$ and $k = 3$, combined with a small number of sub-steps ($2 \le m \le 10$). The number of sub-steps is given by the grid refinement ratio.

Consider first the case with $k = 2$ (second order Adams) and $m = 2$ (two fast sub-steps). The method(5)–(6) is referred as MAB2(2) and reads

$$\begin{aligned}
z_{n-1} &= z_{n-2} + \frac{3h}{2} g\left(y_{n-2}, z_{n-2}\right) - \frac{h}{2} g\left(y_{n-4}, z_{n-3}\right) , \\
z_{n} &= z_{n-1} + \frac{3h}{2} g\left(y_{n-2}, z_{n-1}\right) - \frac{h}{2} g\left(y_{n-4}, z_{n-2}\right) , \\
y_{n} &= y_{n-2} + \frac{3h}{2}\Big(f\left(y_{n-2}, z_{n-1}\right) + f\left(y_{n-2}, z_{n-2}\right)\Big) \\
&\qquad - \frac{h}{2}\Big(f\left(y_{n-4}, z_{n-2}\right) + f\left(y_{n-4}, z_{n-3}\right)\Big).
\end{aligned}$$

For the case with $k = 2$ (second order Adams) and $m = 3$ (three fast sub-steps) the MAB2(3) method (5)–(6) reads:

$$\begin{aligned}
z_{n-2} &= z_{n-3} + \frac{3h}{2} g\left(y_{n-3}, z_{n-3}\right) - \frac{h}{2} g\left(y_{n-6}, z_{n-4}\right) , \\
z_{n-1} &= z_{n-2} + \frac{3h}{2} g\left(y_{n-3}, z_{n-2}\right) - \frac{h}{2} g\left(y_{n-6}, z_{n-3}\right) , \\
z_{n} &= z_{n-1} + \frac{3h}{2} g\left(y_{n-3}, z_{n-1}\right) - \frac{h}{2} g\left(y_{n-6}, z_{n-2}\right) , \\
y_{n} &= y_{n-3} + \frac{3h}{2}\Big(f\left(y_{n-3}, z_{n-1}\right) + f\left(y_{n-3}, z_{n-2}\right) + f\left(y_{n-3}, z_{n-3}\right)\Big) \\
&\qquad - \frac{h}{2}\Big(f\left(y_{n-6}, z_{n-2}\right) + f\left(y_{n-6}, z_{n-3}\right) + f\left(y_{n-6}, z_{n-4}\right)\Big).
\end{aligned}$$

For the case with $k = 3$ (third order Adams) and general m we have MAB3(m) method:

$$\begin{aligned}
\text{For} \qquad & \ell = 1, \cdots m : \\
z_{n-m+\ell} &= z_{n-m+\ell-1} + \frac{23h}{12} g\left(y_{n-m}, z_{n-m+\ell-1}\right)
\end{aligned}$$

$$
\begin{aligned}
& & & -\frac{16h}{12} g\left(y_{n-2m}, z_{n-m+\ell-2}\right) \\
& & & +\frac{5h}{12} g\left(y_{n-3m}, z_{n-m+\ell-3}\right) , \\
y_n &= y_{n-m} + \frac{23h}{12} \sum_{\ell=1}^{m} f\left(y_{n-m}, z_{n-m+\ell-1}\right) \\
& & & -\frac{16h}{12} \sum_{\ell=1}^{m} f\left(y_{n-2m}, z_{n-m+\ell-2}\right) \\
& & & +\frac{5h}{12} \sum_{\ell=1}^{m} f\left(y_{n-3m}, z_{n-m+\ell-3}\right) .
\end{aligned}
$$

We next investigate the conservation, order of accuracy, and stability properties of (5)–(6).

2.2 Conservation Properties of Multirate Adams

Multirate Adams method (5)–(6) is conservative. We have the following formal result.

Proposition 2.1 (Conservation) The method (5)–(6) is conservative in the sense that it preserves the linear invariants of the system.

Proof For analysis we eliminate the intermediate fast steps $z_{n-m+\ell}$ in (6) to arrive at the equivalent formulation

$$
z_n = z_{n-m} + h \sum_{i=1}^{k} \beta_i \left(\sum_{\ell=1}^{m} g\left(y_{n-i\cdot m}, z_{n-m+\ell-i}\right) \right) . \tag{9}
$$

A comparison of the slow method (5) with the fast method (9) reveals that the functions f and g are evaluated with the same arguments and same weights for both the slow and the fast components. Following [6, Proposition 3.2] we consider (4) with a linear invariant of the form

$$
e_F^T f\left(y,z\right) + e_S^T g\left(y,z\right) = 0 , \ \ \forall y,z \quad \Rightarrow \quad e_F^T y(t) + e_S^T z(t) = \text{constant} , \ \forall t ,
$$

where e_F, e_S are fixed weight vectors. Using (5) and (9) we have

$$
\begin{aligned}
e_F^T y_n + e_S^T z_n =& e_F^T y_{n-m} + e_S^T z_{n-m} + \\
& + h \sum_{i=1}^{k} \beta_i \sum_{\ell=1}^{m} \underbrace{\left(e_F^T f\left(y_{n-i\cdot m}, z_{n-m+\ell-i}\right) + e_S^T g\left(y_{n-i\cdot m}, z_{n-m+\ell-i}\right) \right)}_{0} .
\end{aligned}
$$

As a consequence, if the space discretization is conservative then the fully discretized solution (5)–(6) is conservative. A timestepping method that preserves the linear invariants together with a conservative space discretization results in a conservative fully discrete solution. ∎

See [6] for a more in depth analysis.

2.3 Consistency of Multirate Adams

The multirate Adams method (5)–(6) is consistent of order two if the "base" method (2) is at least order two. Order three is not achieved for $m > 1$. We have the following formal result.

Proposition 2.2 (Consistency) If the single rate base Adams method (2) is consistent of (at least) order two, then method the (5)–(6) is consistent of order two.

Proof Consider the following Taylor expansion:

$$\begin{aligned} f\left(y_{n-i\cdot m}, z_{n-m+\ell-i}\right) &= f - imh\, f_y f - (m-\ell+i)h\, f_z g \\ &\quad + \frac{i^2m^2}{2}h^2\left(f_{yy}[f,f] + f_y f_y f\right) \\ &\quad + \frac{(m-\ell+i)^2}{2}h^2\left(f_{zz}[g,g] + f_z g_z g\right) \\ &\quad + \frac{im(m-\ell+i)}{2}h^2\left(2f_{yz}[f,g] + f_z g_y f + f_y f_z g\right), \end{aligned}$$

where all the differentials are evaluated at time n, e.g., $f_y = f_y\left(y_n, z_n\right)$ etc. For the second order derivatives, we use the traditional multilinear notation. As a consequence:

$$\begin{aligned} \sum_{\ell=1}^{m} f\left(y_{n-i\cdot m}, z_{n-m+\ell-i}\right) &= mf - im^2h\, f_y f - \frac{m^2+(2i-1)m}{2}h\, f_z g \\ &\quad + \frac{i^2m^3}{2}h^2\left(f_{yy}[f,f] + f_y f_y f\right) \\ &\quad + \frac{6mi^2+6i(m^2-m)+2m^3-3m^2+m}{12}h^2\left(f_{zz}[g,g] + f_z g_z g\right) \\ &\quad + \frac{2i^2m^2+i(m^3-m^2)}{4}h^2\left(2f_{yz}[f,g] + f_z g_y f + f_y f_z g\right). \end{aligned}$$

For the slow numerical solution (5) we have that

$$y_n - y_{n-m} = h\sum_{i=1}^{k}\beta_i\left(\sum_{\ell=1}^{m} f\left(y_{n-i\cdot m}, z_{n-m+\ell-i}\right)\right)$$

$$
\begin{aligned}
= \quad & m\left(\sum_{i=1}^{k}\beta_i\right) h\, f - m^2\left(\sum_{i=1}^{k} i\beta_i\right) h^2\, f_y\, f \\
& -\left(\left(\sum_{i=1}^{k}\beta_i\right)\frac{m^2-m}{2} + \left(\sum_{i=1}^{k} i\beta_i\right) m\right) h^2\, f_z g \\
& +\frac{1}{2}\left(\sum_{i=1}^{k} i^2\beta_i\right) m^3 h^3 \left(f_{yy}[f,f] + f_y f_y f\right) \\
& +\left(\frac{m}{2}\left(\sum_{i=1}^{k} i^2\beta_i\right) + \frac{m^2-m}{2}\left(\sum_{i=1}^{k} i\beta_i\right)\right. \\
& \left. +\ \frac{2m^3-3m^2+m}{12}\left(\sum_{i=1}^{k}\beta_i\right)\right) h^3 \left(f_{zz}[g,g] + f_z g_z g\right) \\
& +\left(\frac{m^2}{2}\left(\sum_{i=1}^{k} i^2\beta_i\right) + \frac{(m^3-m^2)}{4}\left(\sum_{i=1}^{k} i\beta_i\right)\right) h^3 \left(2f_{yz}[f,g] + f_z g_y f + f_y f_z g\right).
\end{aligned}
$$

Using the order two conditions for the single rate method:

$$
\sum_{i=1}^{k}\beta_i = 1\,, \quad \sum_{i=1}^{k} i\beta_i = \frac{1}{2}\,, \tag{10}
$$

and order three condition

$$
\sum_{i=1}^{k} i^2\beta_i = \frac{1}{3}\,, \tag{11}
$$

we have that the Taylor series of the slow numerical solution reads

$$
\begin{aligned}
y_n - y_{n-m} \quad = \quad & mh\, f - \frac{m^2h^2}{2}\, f_y\, f - \frac{m^2h^2}{2}\, f_z g \\
& +\frac{m^3h^3}{6}\left(f_{yy}[f,f] + f_y f_y f\right) \\
& +\frac{m^3h^3}{6}\left(f_{zz}[g,g] + f_z g_z g\right) \\
& +\frac{(3m^3+m^2)}{24} h^3 \left(2f_{yz}[f,g] + f_z g_y f + f_y f_z g\right) \\
& +O\left(h^4\right)\,.
\end{aligned}
$$

The Taylor series of the exact slow solution about t_n reads

$$\begin{aligned} y(t_n) - y(t_n - mh) &= mh\, f - \frac{m^2h^2}{2} f_y\, f - \frac{m^2h^2}{2} f_z g \\ &\quad + \frac{m^3h^3}{6}\Big(f_{yy}[f,f] + f_y f_y f + f_{zz}[g,g] + f_z g_z g \\ &\quad + 2f_{yz}[f,g] + f_z g_y f + f_y f_z g\Big) + O\left(h^4\right). \end{aligned}$$

We see that the Taylor series of the numerical solution matches the Taylor series of the exact solution up to and including the $O(h^2)$ terms if the second order conditions (10) hold for the base methods. The multirate method is second order for any m if the base method is second order accurate.

When the base method is consistent of order three (11) the coefficients of the $O(h^3)$ terms that involve only y or only z derivatives match the coefficients of the exact solution for any m. However, the coefficient of the $O(h^3)$ term that involves both derivatives in y and in z is different than the exact term: $(3m^3 + m^2)/24 \neq m^3/6$ if $m \neq 1$. The error coefficient of this term increases with the cube of the step size ration m.

A similar Taylor series argument can be made for the fast variable z:

$$\begin{aligned} z_n - z_{n-m} &= mh\, g - \frac{m^2h^2}{2} g_y\, f - \frac{m^2h^2}{2} g_z g \\ &\quad + \frac{m^3h^3}{6}\Big(g_{yy}[f,f] + g_y f_y f\Big) \\ &\quad + \frac{m^3h^3}{6}\Big(g_{zz}[g,g] + g_z g_z g\Big) \\ &\quad + \frac{(3m^3+m^2)}{24} h^3\Big(2g_{yz}[f,g] + g_z g_y f + g_y f_z g\Big) \\ &\quad + O\left(h^4\right), \\ z(t_n) - z(t_n - mh) &= mh\, g - \frac{m^2h^2}{2} g_y\, f - \frac{m^2h^2}{2} g_z g \\ &\quad + \frac{m^3h^3}{6}\Big(g_{yy}[f,f] + g_y f_y f + g_{zz}[g,g] + g_z g_z g \\ &\quad + 2g_{yz}[f,g] + g_z g_y f + g_y f_z g\Big) + O\left(h^4\right). \end{aligned}$$

■

Remark 5. We can therefore consider second order methods of the form (5)–(6) with any number of steps. The AB2 method

$$w_n = w_{n-1} + \frac{3}{2} h\, f\Big(w_{n-1}\Big) - \frac{1}{2} h\, f\Big(w_{n-2}\Big), \tag{12}$$

uses the smallest number of steps ($k = 2$) and will be the focus of the remaining part of this paper. In principle, one can consider more steps if needed for better stability.

Remark 6. The results on conservation (Proposition 2.1) and on order conditions (Proposition 2.2) hold for implicit Adams methods as well. In this case $\beta_0 \neq 0$ and the summations in the proofs go from $i = 0$ to $i = k$. To illustrate the computational pattern of an implicit multirate method (5)–(6), consider the trapezoidal method with $\beta_0 = \beta_1 = 1/2$. The multirate trapezoidal method reads

$$y_n = y_{n-m} + \frac{h}{2}\sum_{\ell=1}^{m} f\left(y_n, z_{n-m+\ell}\right) + \frac{h}{2}\sum_{\ell=1}^{m} f\left(y_{n-m}, z_{n-m+\ell-1}\right), \quad (13)$$

$$z_{n-m+\ell} = z_{n-m+\ell-1} + \frac{h}{2}g\Big(y_n, z_{n-m+\ell}\Big) + \frac{h}{2}g\Big(y_{n-m}, z_{n-m+\ell-1}\Big), \quad (14)$$
$$\ell = 1, \cdots, m\,.$$

The slow solution y_n and the fast solutions $z_{n-m+\ell}$ for all $\ell = 1, \cdots, m$ intermediate steps need to be solved *together*, as they are all coupled in the large (non)linear system (13)–(14). Our focus in what follows in on explicit Adams-Bashforth methods.

2.4 Stability of Multirate Adams Methods

We next consider the nonlinear stability properties of the multirate Adams methods. It has been shown by Hundsdorfer et al. [17] that the single rate AB2 method (12) is strong stability preserving under a timestep restriction if a proper initialization procedure is used.

The stability results in this paper rely on the assumption that the multirate linear multistep method is properly initialized. It is convenient and customary to start the SSP multistep method with an SSP Runge-Kutta method such that all steps satisfy (3). The same approach can be employed to start the multirate method. A single rate SSP Runge-Kutta method with (a small) step h/r can be used to fill in the solution components required by the multirate method ($0 \leq n \leq k\,m$). The factor r is an integer, needed to ensure that the solution remains SSP during the Runge-Kutta initial integration:

$$\left\|\left[\begin{array}{c} y_{n+\frac{i+1}{r}h} \\ z_{n+\frac{i+1}{r}h} \end{array}\right]\right\| \leq \left\|\left[\begin{array}{c} y_{n+\frac{i}{r}h} \\ z_{n+\frac{i}{r}h} \end{array}\right]\right\| \leq \left\|\left[\begin{array}{c} y_0 \\ z_0 \end{array}\right]\right\|, \; 0 \leq n \leq k\,m\,, \; 0 \leq i \leq r-1\,, \quad (15)$$

where $\|\circ\|$ is any norm or the TV semi-norm. If $r = 1$ then the Runge-Kutta method takes the same timestep as the Adams method for the fast

component. The Runge-Kutta offers all the values of y and z needed to start the multirate scheme.

Consider the following vector representation of (5)–(6) at timestep $n \geq 2m$:

$$w_n = \begin{bmatrix} y_n \\ z_n \end{bmatrix} = \begin{bmatrix} y_{n-1} \\ z_{n-1} \end{bmatrix} + h \sum_{i=1}^{k} \beta_i \begin{bmatrix} f\Big(y_{(M-i)\cdot m}, z_{n-i}\Big) \\ g\Big(y_{(M-i)\cdot m}, z_{n-i}\Big) \end{bmatrix}, \tag{16}$$

where

$$(M-1)m < n \leq Mm \;\; \Rightarrow \;\; M = (n-1) \div m + 1\,,\; n = (M-1)m + \ell\,,\; 1 \leq \ell \leq m\,.$$

Representation (16) can be expressed as a perturbed linear multistep method with the arguments of f and g evaluated at each fast time instance, $n-i$, $i = 1 \ldots k$:

$$\begin{bmatrix} y_n \\ z_n \end{bmatrix} = \begin{bmatrix} y_{n-1} \\ z_{n-1} \end{bmatrix} + h \sum_{i=1}^{k} \beta_i \begin{bmatrix} f\Big(y_{n-i}, z_{n-i}\Big) \\ g\Big(y_{n-i}, z_{n-i}\Big) \end{bmatrix} + d_n\,, \tag{17}$$

where the perturbation d_n is given by

$$d_n = h \sum_{i=1}^{k} \beta_i \left(\begin{bmatrix} f\Big(y_{(M-i)\cdot m}, z_{n-i}\Big) \\ g\Big(y_{(M-i)\cdot m}, z_{n-i}\Big) \end{bmatrix} - \begin{bmatrix} f\Big(y_{n-i}, z_{n-i}\Big) \\ g\Big(y_{n-i}, z_{n-i}\Big) \end{bmatrix} \right). \tag{18}$$

Next we investigate the nonlinear stability properties of the multirate method (17).

We begin by recalling Theorem 4.1 of Hundsdorfer and Ruuth [16]. Consider (2) with appropriate starting conditions (as specified in [16]) and with the appropriate timestep restrictions $h \leq h_{\max}$. The solution of a perturbed linear multistep method:

$$w_n = w_{n-1} + h \sum_{i=1}^{k} \beta_i F\Big(w_{n-i}\Big) + d_n\,,$$

where d_n is the perturbation at time t_n, is bounded by

$$\|w_n\| \leq V \|w_0\| + (n-k+1) S \max_{k \leq j \leq n} \|d_j\|\,, \quad n \geq k\,, \tag{19}$$

where V is a constant independent of n, and S is a method specific constant ($S \leq 3/2$ for AB2). We next analyze the stability of the MAB2 solution and start with the following technical Lemmas.

Lemma 2.3 If method (16) is linearly stable for the given h and if f and g are *Lipschitz continuous* for a given norm $\|\circ\|$ with Lipschitz constant L, then $\|d_n\| \in O(h)$.

Proof The step size h is chosen such that the method (5)–(6) is linearly stable and therefore $\|y_n\| \in O(1)$. The functions f and g are Lipschitz continuous with respect to the norm under consideration. It follows that

$$\begin{aligned}
\|d_n\| &= h \left\| \sum_{i=1}^{k} \beta_i \left[\begin{pmatrix} f \\ g \end{pmatrix} \left(y_{(M-i)\cdot m}, z_{n-i} \right) - \begin{pmatrix} f \\ g \end{pmatrix} (y_{n-i}, z_{n-i}) \right] \right\| \\
&\leq h \cdot L \cdot \sum_{i=1}^{k} \left| \beta_i \right| \cdot \underbrace{\left\| y_{(M-i)\cdot m} - y_{n-i} \right\|}_{O(1)} \\
&\leq \text{constant} \cdot h \\
\|d_n\| &\in O(h) \,.
\end{aligned}$$

∎

Note that in the above argument, the (flux) functions (f and g) are smooth with respect to the solutions (y and z), but the solutions need not be smooth in space.

We remark that Lemma 2.3 also includes the case in which f, g, y, and z are smooth.

Lemma 2.4 If method (16) is linearly stable for the given h and if $f,\ g \in C^2$, y and z are continuous in space, and $\| \circ \|_{TV}$ is the TV semi-norm, then $\|d_n\|_{TV} \in O(h^2)$.

Proof We start with the representation (18):

$$\begin{aligned}
\|d_n\|_{TV} &= h \left\| \sum_{i=1}^{k} \beta_i \begin{pmatrix} f \\ g \end{pmatrix} \left(y_{(M-i)\cdot m}, z_{n-i} \right) - \begin{pmatrix} f \\ g \end{pmatrix} (y_{n-i}, z_{n-i}) \right\|_{TV} \qquad (20) \\
&\leq h \sum_{i=1}^{k} \left| \beta_i \right| \left\| \begin{pmatrix} f \\ g \end{pmatrix} \left(y_{(M-i)\cdot m}, z_{n-i} \right) - \begin{pmatrix} f \\ g \end{pmatrix} (y_{n-i}, z_{n-i}) \right\|_{TV} .
\end{aligned}$$

Denote all solution in pairs in (20) with

$$u_i = \begin{bmatrix} y_{(M-i)\cdot m} \\ z_{n-i} \end{bmatrix}, \quad v_i = \begin{bmatrix} y_{n-i} \\ z_{n-i} \end{bmatrix}, \text{ and } F = \begin{pmatrix} f \\ g \end{pmatrix},$$

and consider index j as the space index with $F_j(\circ)$ being the function evaluated at space index j. Further we denote by δ^- the shift operator in space by one grid point, $\delta^-(w_n)_j = (w_n)_{j-1}$. We assume that $F_{j+1}(w) = F_j(\delta^- w)$, i.e., the same space discretization scheme is applied throughout

the grid. Then the TV semi-norm reads

$$\|F(u_i) - F(v_i)\|_{TV} = \sum_j \left| F_{j+1}(u_i) - F_j(u_i) - \left(F_{j+1}(v_i) - F_j(v_i)\right)\right| .$$

Using the mean value theorem with $w_i = \alpha u_i + (1-\alpha)v_i$, $\alpha \in [0,1]$, and under the smoothness assumptions we obtain the following approximation

$$\begin{aligned}
\|F(u_i) - F(v_i)\|_{TV} &= \sum_j \left| F'_{j+1}(w_i)(u_i - v_i) - F'_j(w_i)(u_i - v_i)\right| \\
&= \sum_j \left| F'_j(\delta^- w_i)(u_i - v_i) - F'_j(w_i)(u_i - v_i)\right| \\
&\leq \sum_j \left\| \left(F'_j(\delta^- w_i) - F'_j(w_i)\right)\right\|_\infty \|u_i - v_i\|_\infty \\
&\leq \sum_j \underbrace{\left\| F''_j\left(\beta\, \delta^- w_i + (1-\beta) w_i\right)\right\|_\infty}_{O(1)} \underbrace{\left\|\delta^- w_i - w_i\right\|_\infty}_{O(\Delta x)} \underbrace{\left\|u_i - v_i\right\|_\infty}_{O(h)} \\
\|F(u_i) - F(v_i)\|_{TV} &\in O(h) ,
\end{aligned}$$

where $\beta \in [0,1]$ and the order approximations follow from calculus. The perturbation is then bounded by

$$\begin{aligned}
\|d_n\|_{TV} &\leq h \sum_{i=1}^{k} \left|\beta_i\right| \cdot \|F(u_i) - F(v_i)\|_{TV} \\
&\leq h \cdot C \cdot O(h) \\
\|d_n\|_{TV} &\in O(h^2) ,
\end{aligned}$$

where C is a constant that does not depend on n. ∎

Next, we use Lemmas 2.3 and 2.4 to prove the nonlinear stability results for the multirate method (5)–(6) in different norms.

Proposition 2.5 (Norm Boundedness) If method (16) is linearly stable and let f and g be *Lipschitz continuous* in norm $\|\circ\|$, then the solution w_n is norm bounded:

$$\|w_n\| \leq B ,$$

where B is a constant.

Proof Using Theorem 4.1 from [16] (19) and Lemma 2.3 we have

$$\|w_n\| \leq C\,\|w_0\| + \mathcal{O}(h)\,,$$
$$\|w_n\| \leq V\,\|w_0\| + n\cdot\mathcal{O}(h) \leq B\,,\ \forall n \leq N\,,$$

where C is a constant. ∎

Proposition 2.6 (TVB) If method (16) is linearly stable, f, $g \in C^2$, and y and z are continuous in space, then the TV of the solution w_n remains bounded and the method is TVB:

$$\|w_n\|_{TV} = B\,,$$

where $B > 0$ is a constant.

Proof Using Theorem 4.1 from [16] and Lemma 2.4 we have:

$$\|w_n\|_{TV} \leq C\,\|w_0\|_{TV} + n\mathcal{O}(h^2) = C\|w_0\|_{TV} + \mathcal{O}(h) \leq B\,.$$

∎

We note that even if the formal proofs use smoothness assumptions, in practice, it is desirable to use these methods with discontinuous solutions. Other single rate discretization methods (e.g., WENO) have proofs based on smoothness assumptions; however, they are very successful in practice for solutions with shocks [30, 31, 32].

2.5 Computational Efficiency

In this section we investigate the efficiency speedup of the multirate method under the assumption that the function evaluations carry the bulk of the computational cost. Even if the slow method has formally as many steps as the fast method, these steps are identical away from the interface, and thus no additional calculations are necessary. This means that the slow method really uses large steps away from the interface.

Consider a telescopic application with $R+1$ levels of refinement. The timesteps for each level are $h_j = H/m^j$, $j = 0 \ldots R$. There are L_j grid points at level j. Under these assumptions, the speedup S, for R nested grids is calculated as

$$S = \left(m^R \sum_{j=0}^{R} L_j \right) \Bigg/ \left(\sum_{j=0}^{R} m^j\, L_j \right).$$

Typically, $L_{j+1} \ll L_j$, i.e., only a small part of the grid at a given level is further refined. In this case $S \approx m^R$. We expect the speedup of the multirate scheme to be significantly larger for multi-dimensional problems.

3 Numerical Experiments

Our numerical experiments use RK2a (see [32]) as the starting procedure with the appropriate Courant number to insure linear and nonlinear stability of the initial solution. We next examine a linear PDE – linear advection – and a nonlinear PDE – Burgers' equation.

3.1 The Advection Equation

The one-dimensional advection equation models the transport of a tracer y with the constant velocity u along the x axis

$$\frac{\partial w(t,x)}{\partial t} + u \cdot \frac{\partial w(t,x)}{\partial x} = 0 \,. \tag{21}$$

The spatial discretization method is based on a finite volume approach described in [15, 33]. The method is third order accurate in space on smooth solutions and is positivity preserving with forward Euler timestepping. The flux limited scheme is defined by

$$w_i' = -\frac{1}{\Delta x}\left(F_{i+\frac{1}{2}} - F_{i-\frac{1}{2}}\right), \quad w_i(t) = \frac{1}{\Delta x_i}\int_{x_{i-\frac{1}{2}}}^{x_{i+\frac{1}{2}}} w(t,x)\,dx\,, \quad w_i' = \frac{\partial w_i}{\partial t}\,, \tag{22}$$

with the numerical flux defined as

$$F_{i+\frac{1}{2}} = F_i + \frac{1}{2}\phi_{i+\frac{1}{2}}\left(F_i - F_{i-1}\right)\,, \tag{23}$$

where ϕ is a nonlinear limiter function.

The positivity preserving property of forward Euler steps extends to Adams-Bashforth steps under more stringent step size restrictions [17]. For AB2, the theoretical Courant number is 4/9. The experimental CFL for positivity of AB2 solution with first order upwind in space is 0.49 and with the above high resolution scheme is 0.40.

3.1.1 Positivity Test

In this section we apply the MAB2(m) time integration scheme for the linear advection equation. The spatial discretization is positive with Euler timestepping and the AB2 integration scheme is SSP under a specific Courant number, which results in an overall positive scheme.

The computational domain has two distinct regions. The (fast) middle region is discretized in time using $h = H/m$ time ratio, while the left and right (slow regions) use timestep H. This setting is shown in Figures 2 where the vertical dashed lines delimit the time refined (central) region

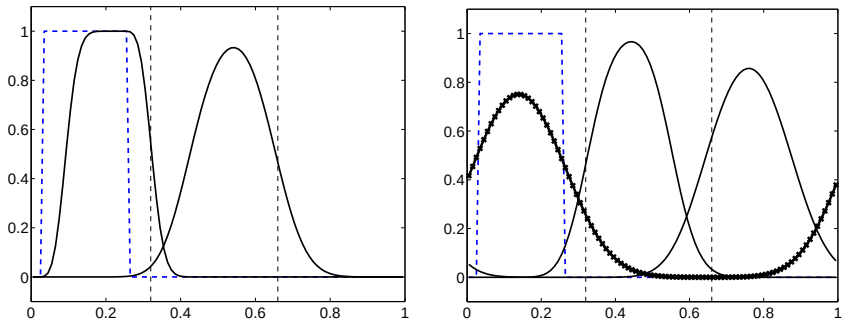

(a) Upwind $t = 0.068,\ 0.4$ (b) Upwind $t = 0.3,\ 0.62,\ 1$

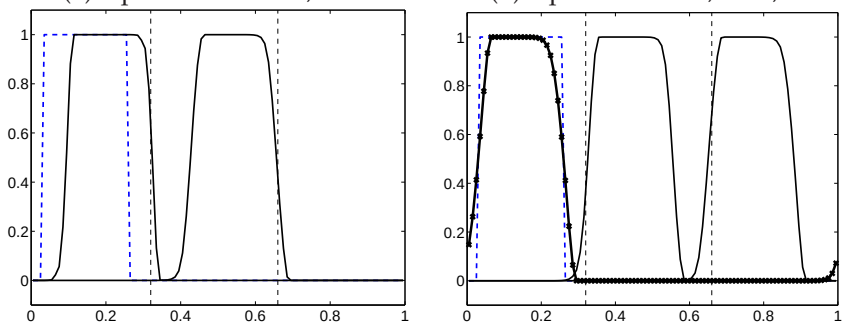

(c) Third order $t = 0.068,\ 0.4$ (d) Third order $t = 0.3,\ 0.62,\ 1.$

Figure 2: The multirate advection solution as the wave passes through the interfaces ($m = 2$). The solution remains positive and there are no geometrical aberrations. The initial step solution is represented with dashed line. The time refined region is in the center of the domain delimited with vertical dashed lines.

from the rest of the domain. For simplicity we consider periodic boundary conditions.

Figures 2 show the advection numerical solution with u=1, 100 grid points, and a Courant number on the slow region of 0.40 for upwind and 0.35 for the third order scheme. The solution is not qualitatively affected by the interface.

In Table 1 we show the minimum, maximum, total mass, and the total variation of the solution for both upwind and third order space discretizations for several time instances (represented in Fig. 2). In both experiments, the solution remains conservative and positive, within the roundoff errors. Moreover, the total variation is non-increasing. The numerical diffusion is more accentuated for the upwind discretization than for the third order as expected.

Time	Upwind				Third Order			
	Min	Max	Mass	TV	Min	Max	Mass	TV
0.00	0.00	1	0.23	2	0.00	1	0.23	2
0.07	0.00	1	0.23	2	-4.85e-17	1	0.23	2
0.30	8.31e-16	0.96	0.23	1.93	-5.69e-17	0.99	0.23	2
0.40	1.52e-10	0.93	0.23	1.86	-6.74e-17	0.99	0.23	1.99
0.62	6.23e-07	0.85	0.23	1.71	-6.14e-17	0.99	0.23	1.99
1.00	0.0001	0.75	0.23	1.50	-3.11e-16	0.99	0.23	1.99
extreme	0.0001	1	0.23	2	-3.20e-16	1	0.23	2

Table 1: The solution minimum, maximum, total mass, and total variation for the advection equation experiments at various time instances and the extreme values for the entire simulation time.

3.1.2 Analysis of Numerical Errors

In this section we analyze the effective (numerical) order of accuracy of the multirate time integration method. For this investigation we use the experiment setting described above and consider the following elements.

The ℓ_q error norms of the numerical solution w, on a grid with spacing Δx_i are computed against a reference solution w^{ref} as follows:

$$\ell_q(w) = \left(\sum_i \Delta x_i \left| w(x_i) - w^{\text{ref}}(x_i) \right|^q \right)^{\frac{1}{q}} .$$

The effective order of the discretization EO_q in q norm is estimated from two numerical solutions with different time resolutions (h and h/γ, $\gamma > 1$), as follows:

$$\text{EO}_q = \log\left(\frac{\ell_q\left(w^{[h/\gamma]}\right)}{\ell_q\left(w^{[h]}\right)} \right) \Big/ \log\left(\frac{1}{\gamma}\right).$$

In our numerical experiments, we use the ℓ_1 and ℓ_2 norms and consider a sine initial solution that is transported half of its period (i.e., 0.5 units in the spatial dimension). The solution is smooth.

For the numerical order validation we use two space discretizations: the upwind and the third order method described above. We consider time refinement while keeping the space grid fixed and compute the error norms ℓ_1^{ODE} and ℓ_2^{ODE}. The reference solution is obtained with a temporal high order numerical approximation, Matlab$^{\text{TM}}$'s RK45 (an explicit Runge-Kutta method, order five with the tight tolerances RelErr=AbsErr=1E-08) [7]. The spatial discretizations are the same for both MAB2 and RK45.

Time fraction	ℓ_1	ℓ_2	EO_1^{ODE}	EO_2^{ODE}
1	1.183e-04	1.315e-04	-	-
2	3.032e-05	3.368e-05	1.964	1.965
4	7.703e-06	8.555e-06	1.977	1.977
8	1.941e-06	2.156e-06	1.989	1.989
16	4.872e-07	5.411e-07	1.994	1.994
32	1.220e-07	1.355e-07	1.997	1.997

Table 2: Effective temporal order of accuracy using MAB2(2) time integration scheme and the upwind method in space. The multirate multistep method does not affect the order of accuracy (in time) of the base AB2 method.

Time fraction	ℓ_1	ℓ_2	EO_1^{ODE}	EO_2^{ODE}
1	1.669e-04	2.380e-04	-	-
2	3.949e-05	5.579e-05	2.079	2.093
4	9.970e-06	1.401e-05	1.986	1.993
8	2.488e-06	3.435e-06	2.002	2.028
16	6.189e-07	8.563e-07	2.008	2.004
32	1.557e-07	2.162e-07	1.991	1.986

Table 3: Effective temporal order of accuracy using MAB2(2) time integration scheme and the third order method in space. The multirate method does not decrease the order of accuracy (in time) of the base (AB2) method.

The error norms are used to approximate directly the time accuracy order EO_1^{ODE} and EO_2^{ODE} for MAB2. In Tables 2 and 3 we show the errors and effective order with the MAB2(2) time integration method and with the first and third order upwind spatial discretizations, respectively. The multirate multistep method has second order as predicted in Sec. 2.3, i.e., the same order as the single rate method AB2.

3.1.3 Computational Efficiency

In this section we validate the theoretical speedup results computed in Section 2.5. We consider the advection equation with a step initial solution using the domain and discretization from above. A small portion of the domain (10% of the total number of grid points) is refined in time with $m = 2$ and $m = 3$. The initial solution is advected for one period (i.e., the final time is one).

In Table 4 we compare the CPU times for the single rate and the multirate integration. The experimental results confirm the theoretical speedup.

Time ratio	Single rate time [sec]	Multirate time [sec]	Experimental speedup	Theoretical speedup
$m = 2$	39.81	19.44	2.04	1.81
$m = 3$	39.81	14.22	2.79	2.50

Table 4: Effective and theoretical computational speedups and timings for MAB2 with $m = 2$ and $m = 3$. The fast region covers 10% of the entire domain. A considerable speedup increase can be obtained for multidimensional applications.

We note that in 2-D and 3-D applications the speedup is expected to be considerably larger, as discussed in Section 2.5. Similarly, more impressive speedups are expected for telescopically nested grids.

3.2 Burgers' Equation

The simplified (inviscid) Burgers' equation is

$$\frac{\partial w(t,x)}{\partial t} + \frac{\partial}{\partial x}\Big(\frac{1}{2}w(t,x)^2\Big) = 0\,.$$

The numerical experiments are based on a third order TVD flux limited scheme for the spatial discretization and MAB2 for the time integration. The discretization is based on the high resolution schemes developed by Osher and Chakravarthy [4, 5, 26, 27]. In their approach the flux $\mathrm{F}(w_{j+1}, w_j)$ is a scalar numerical flux defined for an E-scheme [5]. The following

$$df^-_{j+\frac{1}{2}} = \mathrm{F}(w_{j+1}, w_j) - F(w_j), \text{ and} \tag{24}$$

$$df^+_{j+\frac{1}{2}} = F(w_{j+1}) - \mathrm{F}(w_{j+1}, w_j), \tag{25}$$

represent the positive and negative flux difference on the cell face. With (24)-(25), the following numerical flux is considered

$$F_{j+\frac{1}{2}} = \mathrm{F}(w_{j+1}, w_j) - \Big[\frac{1}{6}\widetilde{df}^-_{j+\frac{3}{2}} + \frac{1}{3}\overline{df}^-_{j+\frac{1}{2}}\Big] + \Big[\frac{1}{3}\widetilde{df}^+_{j+\frac{1}{2}} + \frac{1}{6}\overline{df}^+_{j-\frac{1}{2}}\Big], \tag{26}$$

$$\mathrm{F}(w_{j+1}, w_j) = \frac{1}{2}\Big(F(w_{j+1}) + F(w_j)\Big) - \frac{1}{2}\Big(df^+_{j+\frac{1}{2}} + df^-_{j+\frac{1}{2}}\Big),$$

where $f^\pm$ are the negative and positive flux contributions, $\widetilde{df}^\pm$ and $\overline{df}^\pm$ represent their flux limited form and are defined below. The unlimited (flux) scheme is given by $\overline{df}^\pm = df^\pm$ and $\widetilde{df}^\pm = df^\pm$. The limited fluxes are

defined as follows

$$\widetilde{df}^{-}_{j+\frac{3}{2}} = \text{minmod}\left[df^{-}_{j+\frac{3}{2}},\, b\,df^{-}_{j+\frac{1}{2}}\right], \qquad \overline{df}^{-}_{j+\frac{1}{2}} = \text{minmod}\left[df^{-}_{j+\frac{1}{2}},\, b\,df^{-}_{j+\frac{3}{2}}\right],$$
$$\widetilde{df}^{+}_{j+\frac{1}{2}} = \text{minmod}\left[df^{+}_{j+\frac{1}{2}},\, b\,df^{+}_{j-\frac{1}{2}}\right], \qquad \overline{df}^{+}_{j-\frac{1}{2}} = \text{minmod}\left[df^{+}_{j-\frac{1}{2}},\, b\,df^{+}_{j+\frac{1}{2}}\right],$$

where

$$\text{minmod}\left[x, y\right] = \text{sign}(x)\cdot\max\left[0,\, \min\left[|x|,\, y\,\text{sign}(x)\right]\right], \qquad 1 \le b \le 4.$$

The flux limited method is TVD with forward Euler timestepping. This property extends to Adams-Bashforth steps with more stringent timestep restrictions and a proper initialization. Additional information can be found in [5, 17, 22]. Our numerical experiments confirm that these properties extend to MAB2 with the proper initialization as predicted by our theoretical results. The experimental Courant number for TVD of MAB2 with the above scheme is 0.42.

3.2.1 Nonlinear Stability Experiment

In this section we apply the MAB2 with $m = 3$ time integration scheme for Burgers' equation using the spatial discretization described above. The computational domain is identical to the one described in Section 3.1.1. The initial profile is a square wave and the initial Courant number chosen for this experiment is 0.35 for the initial solution. Note that the Courant number is proportional to the solution magnitude and in this case it decreases over time.

The spatial discretization scheme is TVD and stable under the chosen CFL with forward Euler timestepping and AB2. Figure 3.(a) shows the initial profile advanced in time at different instances. We remark that the solution is not qualitatively affected by the interface.

The time integration scheme, MAB2, with $m = 3$ keeps a bounded total variation. In Figure 3.(b) and (c) we show the time series of the total variation and TV difference (between successive steps), i.e., $\|w_n\|_{TV}$ - $\|w_{n-1}\|_{TV}$, for the solutions presented in Figure 3.(a). This difference is always negative, and thus the scheme is TVD on this particular example. In Figure 4 we show a typical application for the multirate integration schemes developed in this paper. Note that the "magnitude" of the solution also represents its speed and hence the CFL condition can be estimated directly from the solution profile. The initial profile represented by a dashed line, violates the CFL condition. The "fast" area ($m = 3$) is redefined dynamically as the solution evolves in time. The fast area at different times is illustrated in 4 with solid horizontal lines on top of the solution The CFL condition is locally satisfied on the entire domain and the solution remains wiggle-free.

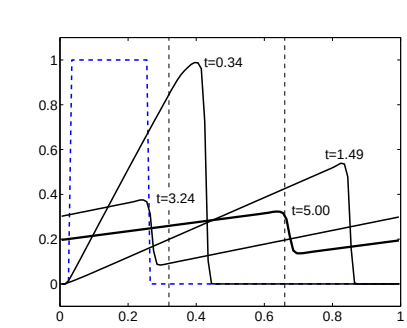

(a) Time evolution

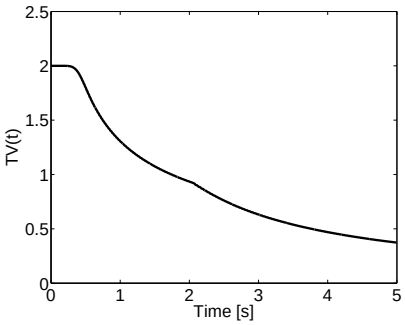

(b) Total variation

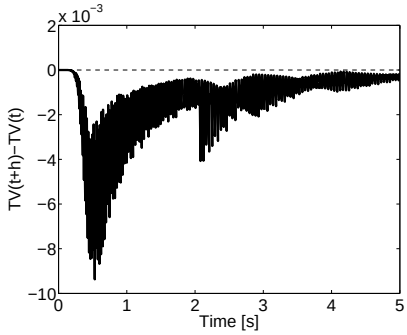

(c) TV during each step

Figure 3: Representation of (a) Burgers' solution at different times with the initial profile dashed. The wave passes through the slow and fast interfaces (dashed vertical lines). The solution remains (b,c) TVD and there are no geometrical aberrations as the solution passes through the interfaces.

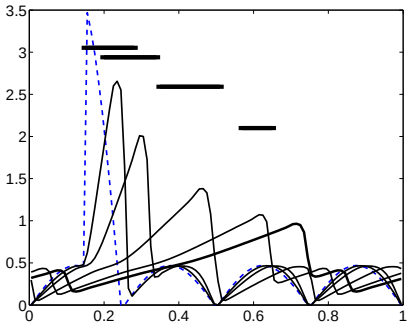

Figure 4: Representation of Burgers' solution using time refinement with $m = 3$ at different instances; time refined regions are represented as horizontal solid lines on top of the solution.

Time fraction	ℓ_1	ℓ_2	EO_1^{ODE}	EO_2^{ODE}
1	2.656e-05	4.269e-05	-	-
2	6.217e-06	9.664e-06	2.095	2.143
4	1.364e-06	2.053e-06	2.188	2.235
8	3.433e-07	5.169e-07	1.990	1.990
16	8.623e-08	1.298e-07	1.993	1.994
32	2.152e-08	3.239e-08	2.003	2.002

Table 5: Effective temporal order of accuracy using MAB2(3) time integration scheme and the third order method in space. The multirate multistep method does not affect the order of accuracy.

3.2.2 Effective Order Test

In this section we investigate the effective order of accuracy for Burgers' equation using the same procedure as in Sec. 3.1.2. We consider an initial sine profile and advance it in time from 0 to 0.1 seconds. The time refined region uses a timestep of $h = H/3$ (i.e., m=3). The results are shown in Table 5. As predicted by the theory, the order of accuracy is two, same as for the single rate method; therefore, multi-stepping does not affect accuracy.

4 Conclusions

Adaptive simulations of conservation laws refine the spatial grid to obtain the target accuracy. Due to the CFL restrictions, finer local grids lead to smaller global timesteps for the entire simulation. Therefore, mesh refinement is accompanied by a considerable increase in the computational time. Moreover, even for fixed grid simulations, the wave speeds may vary considerably across the entire domain and the global timestep is restricted by the fastest wave speed. In both cases, the majority of the variables are solved with a timestep much smaller than necessary.

Multirate integration schemes use different timesteps for distinct components of the solution; in particular, they allow to use different timesteps in different parts of the domain when simulating hyperbolic systems. Each sub-domain takes a timestep that matches the local characteristic time scale of the solution. The goal is to have the desired accuracy and stability under only local CFL restrictions.

In this paper we develop multirate linear multistep Adams-Bashforth methods. The proposed time discretizations are (1) second order accurate, (2) conservative, and (3) nonlinearly stable under local CFL timestep restrictions. Nonlinear stability properties include norm and total variation boundedness. Note that current multirate methods with these properties,

available in the literature, are at most first order accurate. The proposed multirate family of schemes can be extended telescopically to accommodate an arbitrary number of partitions (time scales), with arbitrary step size ratios between partitions.

Two test problems are used to illustrate the theory. In both problems we used MAB2 with different timestep ratios. The first test is the linear advection equation. Under local CFL conditions, the integration is linearly stable and conservative, and the solution remains positive and free of spurious oscillations. The second test is the inviscid Burgers' equation. The wave speed varies significantly in different parts of the domain. Different timesteps that obey the local CFL conditions are used. The numerical solution is conserved and its total variation decreases with time. Note that even if the theoretical results are obtained under smoothness assumptions, in these examples the positivity and TVD properties are preserved for non-smooth solutions. Moreover, we prove TVB while in practice the TVD property is obtained.

Adaptive and automated partitioning methods need to be investigated in order to thoroughly take advantage of the these multirate methods. We shall apply these multirate timestepping algorithms to the solution of large scale 3-D PDEs arising in air quality modeling.

References

[1] J. Andrus, *Numerical solution for ordinary differential equations separated into subsystems*, SIAM Journal of Numerical Analysis, 16 (1979), pp. 605–611.

[2] ——, *Stability of a multi-rate method for numerical integration of ODEs*, Computers & Mathematics with applications, 25 (1993), pp. 3–14.

[3] A. Bartel and M. Günther, *A multirate W-method for electrical networks in state-space formulation*, Journal of Computational Applied Mathematics, 147 (2002), pp. 411–425.

[4] S. Chakravarthy and S. Osher, *Numerical experiments with the Osher upwind scheme for the Euler equations*, AIAA Journal, 21 (1983), pp. 241–1248.

[5] ——, *Computing with high-resolution upwind schemes for hyperbolic equations*, Lectures in applied mathematics, 22 (1985), pp. 57–86.

[6] E. Constantinescu and A. Sandu, *Multirate timestepping methods for hyperbolic conservation laws*, To appear in Journal of Scientific Computing, (2007).

[7] J. Dormand and P. J. Prince, *A family of embedded Runge-Kutta formulae*, Journal of Computational and Applied Mathematics, 6 (1980), pp. 19–26.

[8] C. Engstler and C. Lubich, *Multirate extrapolation methods for differential equations with different time scales*, Computing, 58 (1997), pp. 173–185.

[9] C. Gear and D. Wells, *Multirate linear multistep methods*, BIT, 24 (1984), pp. 484–502.

[10] S. Gottlieb, C.-W. Shu, and E. Tadmor, *Strong stability-preserving high-order time discretization methods*, SIAM Rev., 43 (2001), pp. 89–112.

[11] M. Günther, A. Kværnø, and P. Rentrop, *Multirate partitioned Runge-Kutta methods*, BIT, 41 (2001), pp. 504–514.

[12] M. Günther and P. Rentrop, *Multirate ROW-methods and latency of electric circuits*, Applied Numerical Mathematics, (1993).

[13] E. Hairer, S. Norsett, and G. Wanner, *Solving Ordinary Differential Equations I: Nonstiff Problems*, Springer, 1993.

[14] A. Harten, *High resolution schemes for hyperbolic conservation laws*, Journal of Computational Physics, 49 (1983), pp. 357–393.

[15] W. Hundsdorfer, B. Koren, and M. van Loon, *A positive finite-difference advection scheme*, Journal of Computational Physics, 117 (1995), pp. 35–46.

[16] W. Hundsdorfer and S. Ruuth, *On monotonicity and boundedness properties of linear multistep methods*, Mathematics of Computation, 75 (2006), pp. 655–672.

[17] W. Hundsdorfer, S. Ruuth, and R. Spiteri, *Monotonicity-preserving linear multistep methods*, SIAM Journal on Numerical Analysis, 41 (2003), pp. 605–623.

[18] T. Kato and T. Kataoka, *Circuit analysis by a new multirate method*, Electrical Engineering in Japan, 126 (1999), pp. 55–62.

[19] J. Kraaijevanger, *Contractivity of Runge-Kutta methods*, BIT, 31 (1991), pp. 482–528.

[20] A. Kværnø, *Stability of multirate Runge-Kutta schemes*, International Journal of Differential Equations and Applications, 1 (2000), pp. 97–105.

[21] A. Kværnø and P. Rentrop, *Low order multirate Runge-Kutta methods in electric circuit simulation*, 1999.

[22] C. Laney, *Computational Gasdynamics*, Cambridge University Press, 1998.

[23] H. Lenferink, *Contractivity preserving explicit linear multistep methods*, Numerische Mathematik, 55 (1989), pp. 213–223.

[24] ——, *Contractivity preserving explicit linear multistep methods*, Mathematics of Computation, 55 (1991), pp. 177–199.

[25] R. LeVeque, *Finite volume methods for hyperbolic problems*, Cambridge University Press, 2002.

[26] S. Osher and S. Chakravarthy, *High resolution schemes and the entropy condition*, SIAM Journal on Numerical Analysis, 21 (1984), pp. 955–984.

[27] ——, *Very high order accurate TVD schemes*, Oscillation Theory, Computation, and Methods of Compensated Compactness, IMA Vol. Math. Appl., 2 (1986), pp. 229–274.

[28] J. Rice, *Split Runge-Kutta methods for simultaneous equations*, Journal of Research of the National Institute of Standards and Technology, 60 (1960).

[29] J. Sand and K. Burrage, *A Jacobi waveform relaxation method for ODEs*, SIAM Journal on Scientific Computing, 20 (1998), pp. 534–552.

[30] C.-W. Shu, *Total-variation-diminishing time discretizations*, SIAM Journal on Scientific and Statistical Computing, 9 (1988), pp. 1073–1084.

[31] C.-W. Shu and S. Osher, *TVB uniformly high-order schemes for conservation laws*, Mathematics of Computation, 49 (1987), pp. 105–121.

[32] ——, *Efficient implementation of essentially non-oscillatory shock-capturing schemes*, Journal of Computational Physics, 77 (1988), pp. 439–471.

[33] C. Vreugdenhil and B. Koren, eds., *Numerical Methods for Advection–Diffusion Problems*, vol. 45, Vieweg, 1993.